Experimental determination of the equilibrium Fe isotope fractionation between Fe-aq(2+) and FeSm (mackinawite) at 25 and 2 degrees C

Authors' final draft or 'Post-Print' version. The final version was accepted for publication in Geochimica et Cosmochimica Acta and published by Elsevier (2011)
Cite as: Guilbaud, R, Butler, IB, Ellam, RM, Rickard, D & Oldroyd, A 2011, 'Experimental determination of the equilibrium Fe isotope fractionation between Fe-aq(2+) and FeSm (mackinawite) at 25 and 2 degrees C' Geochimica et Cosmochimica Acta, vol 75, no. 10, pp. 2721-2734.
DOI: 10.1016/j.gca.2011.02.023

Experimental determination of the equilibrium Fe isotope fractionation between Fe^{2+}_{aq} and FeS_m (mackinawite) at 25°C and 2°C.

Romain Guilbaud[a,c,*], Ian B Butler[a,c], Rob M Ellam[b,c], David Rickard[d] & Anthony Oldroyd[d]

[a]*School of Geosciences, University of Edinburgh, Edinburgh, UK*

[b]*Scottish Universities Environmental Research Centre, East Kilbride, UK*

[c]*ECOSSE (Edinburgh Collaborative of Subsurface Science and Engineering). A Joint Research Institute of the Edinburgh Research Partnership in Engineering and Mathematics.*

[d]*School of Earth and Ocean Sciences, Cardiff University, Cardiff, UK*

* Corresponding author. *E-mail address*: R.Guilbaud@sms.ed.ac.uk

ABSTRACT

We report the first experimentally-determined metal isotope equilibrium fractionation factors for a metal sulphide at ambient temperatures and pressures. Mackinawite, referred here as FeS_m (where the subscript m indicates mackinawite), can be a reactive component in diagenetic pyrite formation and the extent of equilibration between FeS_m and dissolved Fe(II) has direct implications the $\delta^{56}Fe$ signatures recorded in diagenetic pyrite. The measured equilibrium Fe isotope fractionation between $Fe(II)_{aq}$ and FeS_m is $\Delta^{56}Fe_{Fe(II)\text{-}FeS}$ = -0.52 ± 0.16 ‰ at 2°C and $\Delta^{56}Fe_{Fe(II)\text{-}FeS}$ = -0.33 ± 0.12 ‰ at 25°C and pH 4. At the experimental pH the equilibrium fractionation factor between all dissolved Fe(II) species and FeSm ($\Delta^{56}Fe_{Fe(II)\text{-}FeS}$) equates to the fractionation factor between Fe^{2+}_{aq} and FeS_m ($\Delta^{56}Fe_{Fe2+\text{-}FeS}$). The measured fractionations are of the same order as other non–redox fractionations measured in low-temperature Fe-C-O systems. We show that at low temperature, the $Fe(II)_{aq}$ – FeS_m system is slowly asymptotic to isotopic equilibrium and consequently, FeS_m is likely to partially conserve kinetically derived isotopic signatures generated on precipitation. Combined with the range of published kinetic fractionations measured on FeS_m precipitation, our data suggest that, subject to the degree of isotope exchange during equilibration, FeS_m can display $\delta^{56}Fe$ compositions encompassing a range of ~ 1.4 ‰.

1. INTRODUCTION

In the past decade, transition metal isotope analyses have become widespread as a means of probing present-day and ancient environmental processes and the evolution of (bio)geochemical cycles. Many of these studies have utilised metal-sulphide isotope systems, and interpreting their results has often been restricted to the lack of provision of experimental data that quantify the direction and extent of isotope fractionations. The iron isotope system applied to Fe sulphides and especially pyrite, the major environmentally significant transition metal sulphide, is an eloquent example. Fe isotope data reported here are expressed in the conventional per mil notation with respect to the IRMM-014 standard, where $\delta^{56(57)}Fe = [(^{56(57)/54}Fe_{sample}/^{56(57)/54}Fe_{IRMM-014})-1] \times 1000$. Most terrestrial igneous rocks have very homogeneous $\delta^{56}Fe$ signatures clustered around ~ 0 ‰ (*e.g.* Beard and Johnson, 2004; Dauphas and Rouxel, 2006, for review). Fe isotope excursions (where $\delta^{56}Fe$ varies from ~ +1 ‰ to ~ -3.5 ‰) recorded in Precambrian, anoxic, sulphidic sediments (*e.g.* Rouxel et al., 2005) in which pyrite is the dominant Fe-S species, raised divergent interpretations (*e.g.* Archer and Vance, 2006; Rouxel et al., 2005). Various theories have been proposed to explain those variations (*e.g.* Yamaguchi et al., 2005; Anbar and Rouxel, 2007; Johnson et al., 2008). Major questions are whether or not i) pyrite is a passive recorder of the Fe(II) reservoir; ii) its formation is accompanied by significant Fe isotope fractionation; and iii) microbial activity is responsible for those Fe isotope signatures. To date, none of the proposed mechanisms responsible for the observed variations has experimentally been confirmed.

Experimental data on aqueous Fe species, Fe-oxides and Fe-carbonates have been documented and demonstrate that the largest Fe isotope fractionations are produced during redox reactions in both biologically mediated (Brantley et al., 2001,2004; Anbar, 2004; Johnson et al., 2004; Beard et al., 1999,2003; Icopini et al., 2004; Croal et al., 2004) and abiotic systems (Anbar et al., 2000; Bullen et al., 2001; Skulan et al., 2002 Brantley et al., 2004; Welch et al., 2003; Matthews et al., 2004; Teutsch et al., 2005; Jang et al., 2008, Handler et al., 2009; McAnena, 2009, Beard et al., 2010). Smaller, but significant fractionations have been seen in abiotic non-redox reactions (Wiesli et al., 2004;

Wiedehold et al., 2006; Dideriksen et al., 2008; Mikutta et al., 2009), including the ligand-exchange process involved in mackinawite (FeS_m) formation (Butler et al., 2005).

FeS_m is a metastable nanoparticulate tetragonal Fe(II) monosulphide (Rickard and Luther, 2007, and references therein) and is a potential reactive iron source in pyrite forming systems since FeS_m dissolves and reacts to form pyrite (Rickard and Luther, 1997). Isotopic mobility and potential equilibration between FeS_m and coexisting dissolved Fe(II) species ($Fe(II)_{aq}$) have direct implications for the ultimate Fe isotope signature of pyrite preserved in geological record. Rickard (2006) showed that in acidic environments, the pH dependent solubility of FeS_m is described by $\log K_{sp1} = \log\{Fe^{2+}\} + \log\{H_2S\} - 2\log\{H^+\} \geq 3.5$. In neutral to alkaline environments, FeS_m solubility is pH independent. Total dissolved Fe(II) is dominated by FeS clusters, FeS^0_{aq}, and $\log K_{sp2} = \log\{FeS^0_{aq}\} = -5.7$. For all natural environments where its solubility product is exceeded, FeS_m is the first Fe-S phase to precipitate.

The kinetics and mechanisms of FeS_m formation from aqueous solutions have been reported (Rickard, 1995) and the fast precipitation process is a ligand-exchange reaction consistent with Eigen-Wilkins kinetics in which the rate of formation is determined by the exchange of water and sulphide molecules in hexaqua iron(II) sulphide between the outer sphere and the inner sphere complexes. FeS_m is readily formed in aqueous solutions as a nanoparticulate precipitate (Wolthers et al., 2003; Michel et al., 2005; Ohfuji and Rickard, 2006; Rickard et al., 2006; Jeong et al., 2008). FeS_m nucleation involves the initial formation of FeS^0_{aq} (Theberge and Luther, 1997; Luther and Rickard, 2005).

Since FeS_m formation is fast and readily reversible (*cf.* Rickard, 2006), the FeS_m-$Fe(II)_{aq}$ system is particularly suitable for equilibrium fractionation studies. However, experimental measurements are limited to kinetic fractionation factors (Butler et al., 2005). Butler and co-workers (Butler et al., 2005; Guilbaud et al., 2010a) observed that the precipitation of FeS_m nanoparticles from Fe(II) solution at low temperature is accompanied by a kinetic fractionation ranging from $\Delta^{56}Fe_{Fe(II)\text{-}FeS} \sim +0.9$ to ~ 0.3 ‰ (where $\Delta^{56}Fe_{A\text{-}B} = \delta^{56}Fe_A - \delta^{56}Fe_B$). After rapid precipitation, isotope exchange occurs between FeS_m and $Fe(II)_{aq}$, and its rate slows down to asymptote to a steady state after 168 hours, at which point FeS_m remains depleted in heavier isotopes with respect to $Fe(II)_{aq}$. The observation that during

precipitation, FeS_m incorporates the lighter isotopes (Butler et al., 2005, Guilbaud et al., 2010a) has often been generalised to pyrite, assuming that a fractionation of a similar magnitude would be recorded during pyrite formation (Severmann et al., 2006; Matthews et al., 2004; Rouxel et al., 2005; Archer and Vance, 2006; Yamagushi et al., 2005). This resulted in various interpretations for the highly ^{56}Fe depleted Archean pyrite signatures. Furthermore, the calculated reduced partition factor ($\beta^{56/54}$) for the Fe^{2+}-pyrite couple, described by Eq. 1, predict ^{56}Fe enrichment in pyrite (*e.g.* Polyakov et al., 2000; Polyakov and Mineev, 2007; Blanchard et al., 2009):

$$10^3 \ln \alpha^{56/54}_{Fe^{2+}-pyrite} = 10^3 \ln \beta^{56/54}_{Fe^{2+}} - 10^3 \ln \beta^{56/54}_{pyrite} \qquad (1)$$

where α stands for the fractionation factor and β for the reduced partition factor.

Butler et al. (2005) noted that even at steady state, the observed $\Delta^{56}Fe_{Fe(II)-FeS}$ did not necessarily represent isotopic equilibrium. Their arguments were based on the fact that i) FeS_m is a sparingly soluble mineral (Rickard, 2006) and isotopic exchange is likely to happen *via* dissolution-precipitation between the mineral surface and the solution rather than the bulk mineral and the solution; and ii) the temperature independence within the range 2-40°C which supports kinetic effects rather than equilibrium. Formation and dissolution of FeS_m is kinetically anisotropic (*i.e.* the rate of dissolution does not equate the rate of precipitation), and the dissolution kinetics are inhibited by transport of reaction components through the diffusion boundary layer (*cf.* Rickard and Sjoberg, 1983). Extrapolations of kinetic isotope fractionations to equilibrium values gave unreasonably large apparent equilibrium factors for O isotope studies (Matsuhisa et al., 1978). Matsuhisa et al. (1978) developed the three-isotope method to overcome this problem and determine experimentally equilibrium isotope fractionations.

In this contribution, we use the three isotope method to determine experimentally the equilibrium Fe isotope fractionation between Fe^{2+}_{aq} and FeS_m. We assess whether or not isotopic equilibrium can be rapidly reached at low temperatures in the aqueous Fe-S system and we discuss our results in terms of computationally derived data and implications of sedimentary pyrite formation. So far, only one other experimental data has been published on Fe isotope fractionations occurring within the Fe-S system (Butler et al., 2005). Schuessler et al. (2007) studied the equilibrium fractionation between

pyrrhotite and silicate melts. Our results are the first reported experimental equilibrium metal isotope fractionation in any metal sulphide aqueous system.

2. METHODS

2.1. Reagents

Experiments were performed at Cardiff University under oxygen free conditions (<1 ppmv O_2) in an MBraun Labmaster 130® re-circulating anoxic chamber. All reagents and acids were analytical grade and solutions were prepared under oxygen free conditions using 18.2 MΩ cm deionised water, sparged with O_2 free grade N_2 for 20-40 min (Butler et al., 1994). Rigorous exclusion of oxygen is essential because FeS_m is pyrophoric and $Fe(II)_{aq}$ itself is prone to oxidation. Iron(II) solution was made by dissolution of Mohr's salt $Fe(NH_4)_2(SO_4)_2 \cdot 6H_2O$ (Sigma Aldrich™) in purged water. Mohr's salt was used for its ability to resist oxidation in solution. Sulphide solution was made by dissolution of $Na_2S \cdot 9H_2O$ (Sigma Aldrich™) in purged water.

2.2. Preparation of ^{56}Fe enriched FeS_m

Two isotopically distinct reservoirs of ^{56}Fe enriched freeze-dried FeS_m (referred as $^{56}FeS_m$) were produced. $^{56}FeS_m$ was prepared by mixing a source of ^{56}Fe enriched iron with $Fe(NH_4)_2(SO_4)_2.6H_2O$. The ^{56}Fe metal, for which the enrichment is given by $m(^{56}Fe)/m(Fe) = 0.997$ and $m(^{57}Fe)/m(Fe) = 0.002$, was supplied by CortecNet™.

An accurately weighed aliquot of ^{56}Fe metal was dissolved in 40 mL hot 3 M HCl, evaporated to incipient dryness to remove the excess acid and the solution was made up to 100 mL. The pH of the solution was determined by an Orion Research EA920® pH meter and was 3 ± 0.1. After N_2 purging, the solution was introduced into the anoxic chamber. In the glove-box, ^{56}Fe solution was mixed with 20 mL 1.4 M hydroxylamine hydrochloride to reduce quantitatively Fe^{3+} to Fe^{2+}. Quantitative

reduction to Fe^{2+} is crucial to prevent formation of S(0) with addition of dissolved HS^-. The $^{56}Fe(II)$ solution was mixed with 250 mL 0.16 M Fe(II) solution made from the dissolution of $Fe(NH_4)_2(SO_4)_2.6H_2O$ in N_2 sparged water. Reduction efficiency was checked by quantifying the residual [Fe^{3+}] in the solution with thiocyanate (*e.g.* Vogel, 1951). An aliquot of the solution was acidified with 2 mL 2M HCl, reacted with 5 mL 4M thiocyanate and made up to 50 mL. The aliquot was analysed with a Perkin Elmer Lambda2® dual beam UV-Vis. Typical response was less than 0.2 ppm for [Fe^{3+}] which represents ~ 0.005‰ of total [Fe].

^{56}FeS was precipitated by mixing the bulk ^{56}Fe solution with equimolar $Na_2S.9H_2O$. The precipitate was filtered with a Buchner filter (Whatman® No. 1 paper) and the filtrate was filtered with a 0.45 μm membrane Millipore™ filter. Freshly precipitated $^{56}FeS_m$ was re-suspended in water and re-filtered three times, freeze-dried for three days (Rickard et al., 2006) and stored in the glove-box. The ^{56}FeS reservoirs produced in this way had isotopic compositions of ~308 ‰ and ~ 2.6 ‰.

2.3. Procedure

In the glove-box, $^{56}FeS_m$ was weighed into a serum bottle, 20 mL 0.05 M Fe(II) solution (pH 4) were added and the serum bottle was sealed with a butyl stopper and an aluminium crimp seal. The mass fraction of Fe in FeS_m and the Fe(II) solution was ~ 0.45:0.55. The serum bottles were placed for ageing on a shaking platform for 25°C experiments and in Haake F6/C25® and Haake DC10/K10® refrigerated circulators for 2°C experiments. After ageing (ageing time up to four months for the 25°C experiment and one month for the 2°C experiments), the solid phase was separated from the aqueous phase by vacuum filtration on a 0.45 μm membrane Millipore® filter. With this filter size, filtrates are clear and filters do not clog (*e.g.* Wolthers et al., 2003; Butler et al., 2005; Rickard, 2006; Rickard et al., 2006; Guilbaud et al., 2010a). The filtrate solution was acidified with concentrated HCl and $^{56}FeS_m$ was dissolved by the addition of a few drops of concentrated HCl. H_2S was allowed to degas from sample in a fume hood.

2.4. Analysis

Samples (Fe(III) in HCl) were taken to dryness and re-dissolved in 5% HNO_3. Total [Fe] in solutions was determined spectrophotometrically with the thiocyanate method (*e.g.* Vogel, 1951). No column chemistry was performed since our samples were experimentally synthesised from analytical grade reagents. $^{56/54}$Fe and $^{57/54}$Fe isotope ratios were measured on a GV IsoProbe (formerly Micromass) multiple-collector inductively coupled plasma mass spectrometer (MC-ICP-MS). The detailed analytical protocol has been described elsewhere (Guilbaud et al., 2010b). The major challenge for accurate and precise measurement of Fe isotopes is the removal of atomic and polyatomic interferences induced by the Ar plasma. This was achieved by increasing the signal-to-background ratio (using high concentration samples and introducing collision gases into the hexapole to decrease and/or remove the interferences) and by stabilising the instrumental mass bias minimising the hexapole potential and decreasing the extraction voltage.

3-10 ppm Fe solutions were introduced into an ApexQ inlet system at 50 µL min^{-1} to maximise the signal to ~0.3 V on mass 54, ~6 V on mass 56 and ~0.02 V on mass 57. Hexapole rf amplitude was set at 50% which enhances transmission of Fe masses. The analysis was run in hard extraction mode (-250 V). 1.8 mL min^{-1} Ar and 2 mL min^{-1} H_2 were introduced into the hexapole collision cell to remove completely ArN^+ on mass 54 and $ArOH^+$ on mass 57 and to decrease ArO^+ on mass 56 to 0.006 V which represents 0.1% of the Fe peak. Cr^+ interferences on mass 54 were monitored on mass 52 but never detected. Analyte size and matrix were the same in samples and standards and the instrumental mass bias was corrected by bracketing each sample with the IRMM-014 standard (*e.g.* Schoenberg and von Blanckenburg, 2005; Guilbaud et al., 2010b). On-peak-zero correction was measured on a 5% v/v HNO_3 solution prior to each Fe solution (samples or standards). Data collection consisted of 5 blocks of 20 5 x 1s integrations, followed by a 4 min rinse in 5% v/v HNO3 + 2% v/v HF. This protocol permits to eliminate memory effects and any Fe build-up in the instrument (e.g. Ellam, 2006; Guilbaud et al., 2010b).

2.5. The three isotope method

The three isotope method (Matsuhisa et al., 1978) is a robust experimental method that allows the determination of equilibrium fractionation factors for elements with three or more stable isotopes. Its principle is to track the evolution of a two end-member system initially far from isotopic equilibrium. It involves the spike-enrichment of one phase in order to shift its isotopic composition away from the terrestrial mass fractionation line (TFL, Fig. 1). The system is then allowed to exchange and equilibrate towards a secondary fractionation line (SFL, or equilibrium fractionation line). Since the SFL is mass dependant, it is parallel to the TFL and lies between the composition of the spiked starting material and the TFL. Any deviation from the bulk composition along the SFL is the measured equilibrium isotopic fractionation between the two phases. In low temperature systems, in which the kinetics are slow, experiments might fail to reach equilibrium, *i.e.* to reach the secondary fractionation line in adequate time for experimental purposes. In such cases, the equilibrium fractionation can be determined from the best fits of the evolution of the phases.

The three isotope method was first used for studies on O (*e.g.* Matsuhisa, 1979; Matthews et al., 1983a,b). More recently, three studies applied this method to the Fe isotope systematics: between oxide and silicate phases at high temperature (Shahar et al., 2008), between chloro-complexes in aqueous solutions (Hill and Schauble, 2008), and between $Fe(II)_{aq}$ and goethite (Beard et al., 2010). Although some workers have used enriched $Fe(II)_{aq}$ solutions, we preferred the solid phase (*i.e.* mackinawite) to be the enriched phase for practical reasons in our experiments. The preparation of clean, contamination-free ^{56}Fe enriched FeS_m is easier experimentally than preparing ^{56}Fe enriched $Fe(II)_{aq}$ from $^{56}Fe(0)$ metal, which would involve the use of metal-complexing species to keep the solution reduced, and which consequently may influence the experimental results.

The equilibrium isotope fractionation between $Fe(II)_{aq}$ and FeS_m, $\Delta^{57}Fe_{Fe(II)\text{-}FeS}$, is the difference between the intersections of the regression lines of all the data set (samples and their duplicates), $\delta^{57}Fe_{Inters.i}$, with the SFL (slope = 0.678). The values of the intersections are given by Eq. 2:

$$\delta^{57}Fe_{Inters_i} = \frac{b - d_i}{c_i - a} \qquad (2)$$

where *a* and *c* are the slopes of the regression lines and the SFL, respectively, *b* and *d* are the intercepts of the regression lines and the SFL, respectively, and *i* stands for the phase of interest.

2.6. Analytical and experimental errors using spiked material in the Fe three isotope system

The analytical precision of our measurements is the reproducibility (2σ, n = 15) obtained by measuring the external Fe standard (Baker™) before and during the analytical run and was ± 0.08 ‰ and ± 0.17 ‰ for δ^{56}Fe and δ^{57}Fe, respectively. Ammonium and sulphate ions present in solutions made from the Mohr's salt were also present in the external Fe Baker™ standard and are thus considered in the given precision. The use of ^{56}Fe spiked material enhances considerably the proportion of mass 56 with respect to other Fe isotopic masses, and therefore the precision on δ^{56}Fe is poorer for spiked samples than for unspiked samples. We analysed seven different aliquots of the starting $^{56}FeS_m$ and found a precision of ± 0.3 ‰ and ± 0.2 ‰ for δ^{56}Fe and δ^{57}Fe, respectively. It is important to note that although the precision is, as predicted, diminished for δ^{56}Fe in the spiked material than for "normal" iron (the precision on δ^{57}Fe being similar), the error remains small when considered within the context of the enrichment of the spiked material for which δ^{56}Fe = 308.3 ‰ and δ^{57}Fe = 5.8 ‰.

Working with metastable nanoparticulate phases that are oxygen sensitive and responsive to small pH variations generally makes experimental errors large compared to analytical errors, as is shown by the duplicate experiments in Table 1 (see discussion below). In order to give conservative uncertainties on the predicted intercepts, we based the total error on the experimental error rather than the smaller analytical error. The uncertainties on $\delta^{56(57)}Fe_{Inters.Fe(II)}$ and $\delta^{56(57)}Fe_{Inters.FeS}$, the upper and lower intercepts between the 95% envelopes on the regression lines, were calculated with the R 2.4.1.® statistical package. The coordinates of the lower and upper 95 % confidence envelopes are calculated conventionally from the regression lines of the entire data set (experimental samples and their duplicates) by Eq. 3 (*e.g.* Ludwig, 1980; Borradaille, 2003):

$$Y = y \pm t_{\alpha/2} s_R \left[\frac{1}{n} + \frac{(x-\bar{x})^2}{\sum (x_i - \bar{x})^2}\right]^{\frac{1}{2}} \qquad (3)$$

where Y is the coordinate of the 95% envelope for each corresponding x on the regression line (y = ax + c), n is the number of data points, $t_{\alpha/2}$ is the value of the t-statistic for a two-tailed test (with n - 2),

the coordinate of the regression line, x_i is the coordinate of data points and $\bar{x}$ is the centroid of the x coordinates. Uncertainties on $\Delta^{56(57)}Fe_{FeS\text{-}Fe(II)}$ are propagated from the uncertainties on $\delta^{56(57)}Fe$ with Eq. 4:

$$\sigma_{\Delta^{56(57)}Fe} = [(\sigma_{\delta^{56(57)}Fe_{lower}})^2 + (\sigma_{\delta^{56(57)}Fe_{upper}})^2]^{\frac{1}{2}} \qquad (4)$$

3. RESULTS

Experimental quality control was performed by monitoring the mass conservation law. At any time during the experiment, the weighed sum of the constituents must equal the isotopic signature of the bulk (Eq. 5, Fig. 2):

$$(f \times \frac{^{56}Fe}{Fe}_{FeS}) + ((1-f) \times \frac{^{56}Fe}{Fe}_{Fe(II)}) = \frac{^{56}Fe}{Fe}_{bulk} \qquad (5)$$

where *f* is the mass fraction of Fe in FeS_m. Note that this equation uses the ratio $^{56}Fe/Fe$ rather than the usual $^{56}Fe/^{54}Fe$. This is due to the fact that unlike ^{18}O in the O system, ^{57}Fe and ^{54}Fe are not trace isotopes with respect to ^{56}Fe. As a result, when mass balancing equations, the error will be significantly increased using usual isotopic ratios (see Criss, 1999; Eq 1.14a-b-c) instead of the (mass of isotope)/(mass of element) ratios. There is a systematic ^{56}Fe enrichment for early experiments, resulting in a shift from mass balance towards higher $\delta^{56}Fe$ values. The likely explanation is that this phenomenon is due to $^{56}FeS_m$ nanoparticles passing through the 0.45 μm filter in the early stages of the experiment, *i.e.* before FeS_m nanoparticles have agglomerated. Note that only 5 % of $^{56}FeS_m$ are required to pass through the filter to shift the $Fe(II)_{aq}$ isotope signature by 10 ‰. It is well known that because of the rapid aggregation of FeS_m nanoparticles into flocs (*e.g.* Wolthers et al., 2003; Ohfuji and Rickard, 2006; Guilbaud et al., 2010a), samples which have aged in suspension are readily trapped on a 0.45 μm filter during vacuum filtration, and form an efficient filter bed such that no FeS_m contribution is seen in the liquid phase. Because imperfectly mass-balanced experiments only concern the very first experiments, it has no observable effect on our extrapolation and predicted fractionations.

3.1. Experiment starting with $\delta^{56}Fe_{FeS}$ ~ 308 ‰ at 25°C and 2°C

Experimental conditions, analytical results and fractionations are presented in Table 1. The experiment starting with $\delta^{56}Fe_{FeS}$ ~ 308 ‰, the bulk composition of the system was 102 ± 3 ‰. The extent of isotopic exchange *F* is given by (Graham et al., 1981; Criss, 1999; Johnson et al., 2002) Eq. 6:

$$F = \frac{\delta^{56}Fe - \delta^{56}Fe_0}{\delta^{56}Fe_{eq} - \delta^{56}Fe_0} \qquad (6)$$

where the subscripts *0* and *eq* stand for *initial* and *equilibrium*, respectively. The advantage when using enriched starting material, is that the value of the equilibrium $\delta^{56}Fe_{eq}$ (~ 300 per mil) is negligible compared to the starting fractionation (~ 300 per mil) and so *F* can be determined precisely.

Fig. 3 describes the evolution of the isotope composition of $Fe(II)_{as}$ and FeS_m as a function of time. Isotopes exchange rapidly within the first 96 hours of ageing. After 96 hours, the exchange slows down and the extent of isotopic exchange is asymptotic to the equilibrium composition. At the end of the experiment, 75 % of isotopes had exchanged at 2°C and 85 % of isotopes had exchanged at 25°C after 4 months ageing. At equilibrium, the three isotope method predicts ^{56}Fe enriched FeS_m with respect to $Fe(II)_{aq}$ for both 25°C and 2°C (Fig. 4). Fe isotope fractionation is larger at 2°C where $\Delta^{56}Fe_{Fe(II)\text{-}FeS}$ = -0.52 ± 0.16 ‰ than at 25°C where $\Delta^{56}Fe_{Fe(II)\text{-}FeS}$ = -0.33 ± 0.12 ‰, although within error, these are strictly the same.

3.2. Experiment starting with $\delta^{56}Fe_{FeS}$ ~ 2.6 ‰ at 25°C

It was assumed that decreasing the initial fractionation between the phases from ~ 308 ‰ to ~ 2.6 ‰ would further narrow down the error bars on the predicted $\Delta^{56}Fe_{Fe(II)\text{-}FeS}$. However in actuality, because the initial compositions of the starting materials are closer, the projection on the SFL is more complicated since both experimental and analytical errors become considerable with respect to the initial fractionation. As a result, although trends were visible on a three isotope plot, the 95 %

confidence envelopes were larger than the predicted fractionation and we could not use those results to further discuss their relevance.

4. DISCUSSION

4.1. Equilibrium fractionation and mechanisms of isotope exchange

The surface chemistry of mackinawite has been established titrimetrically (Wolthers et al., 2005). At pH 4, the surface of FeS_m nanoparticles is positively charged (Wolthers et al., 2005), and therefore Fe^{2+}_{aq} adsorption to the FeS_m surface is insignificant. The constant size of the two different Fe pools (*i.e.* FeS_m and $Fe(II)_{aq}$) and matching mass balance throughout our data set further imply that vacuum filtration quantitatively separated FeS_m from the Fe(II) solution, without any Fe^{2+}_{aq} to be adsorbed and removed from the solution.

At pH 4, the dominant Fe bearing species in the aqueous solution is the hexaqua $Fe[H_2O]_6^{2+}$ (normally referred as Fe^{2+}). Up to ~ 45% of the total dissolved Fe(II) was constituted by the weak outer-sphere SO_4^{2-} ligand complex, $Fe[H_2O]_6SO_4^0{}_{aq}$ (PHREEQC Interactive 2.15.0® gave 45% and Visual MINTEQ 2.61® 42%). In $Fe[H_2O]_6SO_4^0{}_{aq}$, there is no strong Fe-SO_4^{2-} bond. Its participation in $Fe(II)_{aq}$ speciation has thus a negligible effect on the recorded Fe isotope fractionation since the ligand-exchange mechanism occurring remains unaffected. Rickard (2006) showed that under acidic conditions, the equilibrium solubility of FeS_m is described by $\log K_{sp} = \log \{Fe^{2+}\} + \log \{H_2S\} - 2 \log \{H^+\}$. Under neutral to alkaline conditions, the equilibrium solubility of FeS_m is pH independent, and FeS_m dissolves into FeS^0_{aq}. In our experiment, the $Fe(II)_{aq}$ solution was ~ pH 4 and Σ[S(-II)] was 0.05 M. Fig. 5 shows the solubility curves for FeS_m at various Σ[S(-II)]. For Σ[S(-II)] = 0.05 M (this study) the dominant Fe(II) species at pH 4 is Fe^{2+}. For these reasons, the measured equilibrium fractionation between $Fe(II)_{aq}$ and FeS_m equates to the equilibrium isotope fractionation between the chemical species Fe^{2+}_{aq} and FeS_m, $\Delta^{56}Fe_{Fe^{2+}\text{-}FeS}$.

The Fe isotope equilibrium fractionation factor for the exchange reaction between $Fe(II)_{aq}$ and FeS_m (Eq. 7), $\alpha^{56/54}_{Fe(II)_{aq}-FeS_m}$, is 0.99948 ± 0.00002 at 2°C and 0.99967 ± 0.00002 at 25°C, and is given by Eq. 8:

$$^{56}FeS_m + {}^{54}Fe(II)_{aq} = {}^{54}FeS_m + {}^{56}Fe(II)_{aq} \qquad (7)$$

$$\alpha^{56/54}_{Fe(II)_{aq}-FeS_m} = \frac{\delta^{56}Fe_{Fe(II)_{aq}} + 1000}{\delta^{56}Fe_{FeS_m} + 1000} \qquad (8)$$

Our experimentation demonstrates that at equilibrium, the Fe isotope composition of mackinawite is ^{56}Fe enriched with respect to the Fe isotope composition of $Fe(II)_{aq}$. This compares with the kinetic Fe isotope fractionation occurring during FeS_m precipitation (Butler et al., 2005; Guilbaud et al., 2010a) and confirms the conclusion by Butler et al. (2005) who argued that the fractionation observed between FeS_m and $Fe(II)_{aq}$ after 168 hours ageing does not represent equilibrium, but a dynamic steady state. Similarly, Böttcher et al. (1998) came to the same conclusion from their S isotope study on FeS_m precipitation. As mentioned above, Rickard (2006) discussed the solubility of FeS_m and showed that FeS_m is sparingly soluble (pK_{sp} = 3.5 ± 0.25). Butler et al. (2005) suggested that if the mechanism responsible for Fe isotope exchange is dissolution-precipitation, it might be restricted to the mineral-media interface, rather than between whole FeS_m particles and the solution. The rates of precipitation (including nucleation and crystal growth) and dissolution of FeS_m in the FeS_m-H_2O system are well known (*e.g.* Rickard, 1995; Pankow and Morgan, 1980; Rickard and Luther, 2007). The rate of FeS_m dissolution is limited by the transport of components through the particle diffusion boundary layer. This means that the driving force for the rate is essentially the chemical components potential (including Fe^{2+}, S(-II) and H^+) between the FeS_m surface and the solution. As the bulk system approaches equilibrium, the chemical potential becomes smaller and the rate decreases.

Guilbaud et al. (2010a) studied the kinetics of isotope exchange during FeS_m precipitation. They showed that atom exchange between FeS_m and $Fe(II)_{aq}$ is consistent with i) FeS_m nanoparticles that have a core–shell structure, in which case Fe isotope mobility is restricted to exchange between the surface shell and the solution and ii) nanoparticle growth via an aggregation–growth mechanism rather than growth by Ostwald ripening. This means that during the rapid aggregation of FeS_m

nanoparticle flocks, where the non-exchanging core is progressively growing with respect to the surface layer, the rate of isotope exchange continuously slows down. Models presented by Guilbaud et al. (2010a) best fit the isotopic data for FeS_m nanoparticles comprised of a non-exchanging core and a ~ 0.8 nm thick surface layer. Interestingly, studies on growth mechanisms for ZnS nanoparticles (*e.g.* Huang et al., 2003) and other Fe oxides nanoparticulate systems (*e.g.* Waychunas et al., 2005) indicate that in the nanoscale domain, particles are likely to grow *via* aggregation growth rather than *via* Ostwald-ripening. Since the rate of FeS_m dissolution is controlled by the diffusion boundary layer (*e.g.* Pankow and Morgan, 1980; Rickard and Sjoberg, 1983), this tends to further inhibit the rate of approach to equilibrium. Experimentally, after 30 days, Fe isotopic exchange reaches an apparent constant value of ~ 75% and ~ 85% of exchange for 2°C and 25°C, respectively.

4.2. Implications for the equilibrium fractionation at higher pH

For Σ[S(-II)] = 0.05 M and pH > 5.2, FeS_m solubility is pH independent and total dissolved Fe(II) species are dominated by FeS^0_{aq} (Fig. 5). Rickard and Morse (2005) characterised FeS^0_{aq} as multinuclear Fe-S complexes whose stoichiometry ranges from Fe_2S_2 to $Fe_{150}S_{150}$ where the first condense phase precipitates. Luther and Rickard (2005) showed that metal sulphide clusters in the Fe-S, Cu-S and Zn-S systems are structurally congruent with the first-formed solid phase. This leads to a limited energy barrier in the nucleation of these phases from solution. Rickard and Morse (2005) put emphasis on the structural similarity between Fe_2S_2 and FeS_m. This means that the alkaline dissolution of FeS_m into FeS^0_{aq} may involve less Fe-S bond breaking than under acidic conditions, and the majority of Fe(II) is ligated by S both in solution or in the solid phase. For these reasons we propose that under neutral to alkaline conditions, the resulting Fe isotope fractionation between FeS_m and FeS^0_{aq} is small and insignificant. The equilibrium isotope distribution between Fe^{2+}_{aq} and FeS_m is independent of the two FeS_m forming pathways (Eq. 9 and 10):

$$pH < 5.2 : Fe^{2+} + H_2S \rightarrow FeS_m \qquad (9)$$

$$pH > 5.2 : Fe^{2+} + H_2S \rightarrow FeS^0_{aq} \rightarrow FeS_m \qquad (10)$$

Consequently, we propose that $\Delta^{56}Fe_{Fe^{2+}-FeS_m} \approx \Delta^{56}Fe_{Fe^{2+}-FeS^0_{aq}}$, and that the fractionation factor determined in this study is applicable to equilibrium isotope distributions between Fe^{2+}_{aq} and FeS_m at alkaline pH. It is important to emphasise however that, unlike at acid pH, the analytically measured isotopic fractionation between $Fe(II)_{aq}$ (*i.e.* all dissolved Fe(II) species) and FeS_m at neutral to alkaline pH is controlled by the predominance of the FeS^0_{aq} reservoir over the Fe^{2+}_{aq} reservoir. Unfortunately, the low total dissolved Fe concentrations present at alkaline pH make this area difficult to access experimentally.

4.3. Comparison with calculated predictions

To our knowledge, no calculated data exist for the equilibrium fractionation between $Fe(II)_{aq}$ and FeS_m. However, β-factors for aqueous Fe(II), pyrite and the Fe(II) monosulphide troilite have been documented (*e.g.* Schauble et al., 2001; Anbar et al., 2005; Polyakov et al., 2000; Polyakov and Mineev, 2007; Blanchard et al., 2009). Schauble et al. (2001) used published vibrational data and empirical force field model (the Modified Urey-Bradley Force Field model, MUBFF) to estimate the β-factors of numerous Fe(II) and Fe(III) aqueous complexes including hexaqua Fe(II). Jarzecki et al. (2004) and Anbar et al. (2005) used Density Function Theory (DFT) to estimate the β-factors of hexaqua Fe(III) and hexaqua Fe(II). Polyakov and Mineev (2000) and Polyakov et al. (2007) used Mössbauer and inelastic nuclear resonant X-ray scattering (INRXS) data to provide β-factors for pyrite and troilite among others. In order to interpret natural data measured in pyrite, they assumed that the β-factors for mackinawite would be similar to those for troilite, since both are Fe(II) monosulphides. Blanchard et al. (2009) used first principle calculations (Schauble et al., 2001,2006) to discuss the pyrite β-factors given by the technique from Polyakov and co-workers. Fig. 6 shows the temperature dependence of equilibrium $\Delta^{56}Fe_{Fe(II)\text{-sulphide}}$ for pyrite, troilite and our experiment. β-factors for $Fe(II)_{aq}$ are from Schauble et al. (2001) and Anbar et al. (2005). β-factors for pyrite and troilite are from Blanchard et al. (2009), Polyakov and Mineev (2000) and Polyakov et al. (2007). Our results demonstrate that mackinawite and troilite, do not display similar fractionations with respect to

$Fe(II)_{aq}$, which is expected since troilite is a hexagonal Fe(II) monosulphide, with no stability region at low temperature (Rickard and Luther, 2007). Equilibrium enrichment of heavier Fe isotopes in FeS_m is consistent with calculated fractionations for pyrite, which is predicted to incorporate heavy isotopes.

Beard et al. (2010) observed that in general, comparisons between predicted and observed equilibrium fractionations are more consistent for fluid-fluid or mineral-mineral fractionations, rather than for fluid-mineral fractionations. In our case, calculated values for FeS_m β-factors are needed to assess the consistency between theory and experiments.

4.4. Comparison with other experimental studies

Experimental studies have shown that redox processes produce the largest equilibrium Fe isotope fractionations. At 20°C, equilibrium fractionation between $Fe(III)_{aq}$ and $Fe(II)_{aq}$ is ~ +3 ‰ (Johnson et al., 2002; Welch et al., 2003), $\Delta^{56}Fe_{Fe(II)aq\text{-}hematite}$ is ~ - 3 ‰ (Johnson et al., 2002; Skulan et al., 2002; Welch et al., 2003); $\Delta^{56}Fe_{Fe(II)aq\text{-}magnetite}$ is ~ -1.3 ‰ (Johnson et al., 2005), and $\Delta^{56}Fe_{Fe(II)aq\text{-}Fe(III)oxide}$ is ~ -0.9 ‰ (Bullen et al., 2001) and Beard et al. (2010) observed a $\Delta^{56}Fe_{Fe(II)aq\text{-}goethite}$ of ~ -1 ‰. In our experiment, [Fe] was equimolar in FeS_m and $Fe(II)_{aq}$ and no redox process was involved. By analogy, Wiesli et al. (2004) found that the equilibrium fractionation recorded between the non-redox $Fe(II)_{aq}$-siderite couple was ~ 0.48 ‰.

Amongst all transition metal-sulphides, only the behaviour of Cu and Zn isotopes during the precipitation of CuS and ZnS have been studied. CuS precipitates from $Cu(II)_{aq}$ with $\Delta^{65}Cu_{Cu(II)aq\text{-}CuS}$ = 3.06 ± 0.14 ‰ (Ehrlich et al., 2004). Ehrlich et al. (2004) interpreted this result as a redox effect, since the precipitate is reduced to Cu(I)S from the aqueous Cu(II). Like FeS and CuS, Archer (2007) showed that ZnS precipitates from $Zn(II)_{aq}$ with depletion in heavy isotopes ($\Delta^{66}Zn_{Zn(II)aq\text{-}ZnS}$ ~ 0.4 ‰). However, both Ehrlich et al., 2004 and Archer (2007) argued that their values were likely to be kinetic fractionations, CuS and ZnS being significantly less soluble than FeS_m (Ksp_{FeS} = 3.5, (Rickard, 2006); Ksp_{CuS} = 22.2, (Smith et al., 1976); $Ksp_{sphalerite}$ = 10.93, (Dyrssen and Kremling, 1990); where *K*sp values given here are for free hexaqua species and the minerals).

As shown above, after 30 days, Fe isotopic exchange reaches an apparent constant value of ~ 75% and ~ 85% of exchange for 2°C and 25°C, respectively. This compares with the extent of exchange between $Fe(III)_{aq}$ and ferrihydrite nanoparticles, which reaches a maximum of 26 % after 11 days (Poulson et al., 2005). The study by Poulson et al. (2005) was carried out at pH 4.7 with 3 nm ferrihydrite nanoparticles, which is similar to the experimental conditions presented here. Interestingly, the surface of ferrihydrite nanoparticles display a different coordination than the core (Michel et al., 2007) and ferrihydrite nanoparticles may also grow by aggregation growth (Waychunas et al., 2005, Michel et al., 2007) and have a low solubility (K_{sp} = 3-3.4, Schwertman, 1991; Majzlan et al., 2004). We suspect that the origin of the difference between our results and those by Poulson et al. (2005) lies in the large surface layer that promotes atom exchange for transition metal sulphides such as FeS_m and ZnS (Guilbaud et al., 2010a; Zhang et al., 2003).

4.5. Implications for modern natural systems

In marine sedimentary environments, the predominant Fe aqueous species include Fe(III)hydroxyl complexes and Fe^{2+} (Turner et al., 1981). Rickard and Morse (2005) argued that in anoxic, sulphidic environments, Fe(III) species are not significant and concluded that Fe^{2+} is the dominant Fe non-sulphide species under those conditions. In anoxic sedimentary systems isolated from hydrothermal inputs, sources for Fe^{2+} include i) microbial Fe(III) reduction and ii) sulfidation of detrital and/or authigenic highly reactive Fe(III) oxides. Both mechanisms occur at the early stages of diagenesis (Canfield et al., 1992; Poulton and Raiswell 2002). Raiswell and Canfield (1998) showed that modern anoxic/suboxic sediments (*e.g.* Black Sea, Cariaca Basin, Framvaren Fjord) are enriched in highly reactive Fe minerals. Mechanisms for Fe(III) (oxy)hydroxides reduction to Fe(II) are summarised by Wells et al. (1995). Sulfidation of Fe(III) oxyhydroxides, such as goethite, is a fast process (Rickard, 1974; Pyzik and Sommer, 1981; Wei and Osseo-Asare, 1996) that occurs *via* dissolution of the mineral surface, reduction of Fe(III) to Fe(II) and subsequent precipitation of FeS_m. In such environments, the major source for S(-II) is bacterial sulphate reduction, BSR (Raiswell and Berner, 1985) which occurs at a lower rate than Fe reduction (*e.g.* Berner, 1981; Canfield et al., 1992).

Canfield et al. (1992) thus concluded that enrichment in dissolved S(-II) in those environments could only occur after complete sulfidation of Fe(III) oxides. Hence, FeS_m and dissolved Fe(II) should coexist in most environments in which $\Sigma\{S(-II)\}$ and $\Sigma\{Fe(II)\}$ are low (where I.A.P just exceeds Ksp_{FeS}) or where $\Sigma\{Fe(II)\}$ is significantly greater than $\Sigma\{S(-II)\}$, *i.e.* in some marginal environments (costal, deltaic and ridge areas), at the oxic-anoxic interface where sulphide starts forming from sulphate reduction or within the anoxic zone in which H_2S reduces Fe(III) species to Fe^{2+}. In environments in which Fe reduction is extensive, the process may be localised to the boundary between the suboxic and the anoxic zones. Rickard and Morse (2005) noted that FeS_m has been principally observed in Fe rich environments, and rarely observed under "normal" marine conditions. They showed that where FeS_m is present, Fe(II) remains in solution as FeS^0_{aq} or as $Fe(II)_{aq}$ at quite large concentrations. Our results and those from Butler et al. (2005) converge to the same conclusion: in the 2-40°C range, the Fe-S system is slow to attain isotopic equilibrium. This means that for surface environments, the equilibrium number cannot be simply applied, and naturally occurring FeS_m is likely to conserve its slow-exchange kinetic signature. Severmann et al. (2006) measured the Fe isotope compositions of highly reactive Fe in the anoxic margin basins. They documented $\delta^{56}Fe$ values for pore waters, pyrite, and HCl extractable solid phases (*i.e.* FeS_m and $Fe(OH)_3$). Fig. 7 compares the natural measurements with experimentally determined kinetic and equilibrium fractionations between $Fe(II)_{aq}$ and the solids. The data suggest that under diagenetic conditions, the solid products are not in equilibrium with the pore water. Rickard et al. (2007) showed in a cross-over plot that there is no direct link between FeS_m, AVS, and pyrite within the same sediment, since $Fe(II)_{aq}$ can remain dissolved for large temporal and spatial scales in anoxic environments. Therefore, the measured compositions of natural sediments do not necessarily provide fractionation factors between the phases but reflect complicated interaction between the solids and the surrounding liquid.

The temperature dependence of the isotopic exchange suggests that at higher temperatures, the system would reach equilibrium more rapidly. Rouxel et al. (2008) and Bennett et al. (2009) measured the Fe isotope composition of Fe sulphide particles in hydrothermal environments and their results indicate that the composition of those particles is consistent with kinetic fractionations recorded for FeS_m (Butler et al., 2005), in other words, far from the equilibrium data presented here. However,

caution is required with regard to extrapolating these data to temperatures in excess of 100°C, since at those temperatures, mackinawite does not form or transforms into pyrrhotite. Note that hydrothermal Fe sulphide particles can also consist of pyrite and chalcopyrite, for which Fe isotope fractionations upon formation have not been experimentally constrained.

4.6. Implications for ancient sedimentary signatures

In the Fe-S system, Fe is eventually sequestered into pyrite. At least 28 different reactions have been reported for low temperature aqueous synthesis of pyrite (Rickard and Luther, 2007). The use of FeS_m as the Fe(II) reactant for one of these reactions is popular amongst the experimental community since FeS_m first precipitates in protocols, giving sufficient nutrient concentration to produce a useful mass of pyrite. In modern natural environments, as mentioned above, FeS_m as a reactant is limited to inshore and freshwater systems or as a surface product of Fe oxyhydroxide sulfidation. Thus the Fe isotope fractionation recorded during the formation of FeS_m need not influence the Fe isotope composition of pyrite from all geological environments. However, it is possible that FeS_m may have played a major role for diagenetic pyrite formation in sedimentary systems older than ~ 2.4 Ga, in which oceans were $Fe(II)_{aq}$ rich and anoxic (*e.g.* Holland, 1984). Interestingly, it is in those Proterozoic to Archean sediments that pyrite displays the largest Fe isotope excursions. There has been widespread interest in the possible use $\delta^{56}Fe_{pyrite}$ as a paleo-proxy for seawater compositions (*e.g.* Anbar and Rouxel, 2007; Archer and Vance, 2006). But the fractionation involved during the pyrite formation stage is still unknown. Rouxel et al. (2005) showed that Proterozoic pyrites display positive $\delta^{56}Fe$, which is in agreement with the equilibrium calculations for pyrite (Polyakov et al., 2007; Polyakov and Mineev, 2000) and our experimental prediction for mackinawite. However the negative isotopic composition of Archean pyrites implies that further fractionating mechanisms are involved.

The results of this experimentation, along with those reported by Butler et al. (2005), suggest that FeS_m Fe isotope compositions are contained in a ~ 1.4 ‰ range depending on the degree of FeS_m precipitation and equilibration. Depending on the rate of pyrite formation, pyrite might record the

lowest $\delta^{56}Fe$ where Fe_{FeS} is rapidly incorporated into pyrite. Mechanistically, FeS_m dissolves into FeS_{aq} which reacts with S(-II) to form pyrite. The final composition of pyrite will thus depend on the fractionation occurring during FeS_m dissolution, on the extent of mixing with free hexaqua Fe(II) and on the extent of pyritisation. For higher temperatures, *i.e.* during later stages of diagenesis, isotopic equilibration between FeS_m and $Fe(II)_{aq}$ might be reached.

5. CONCLUSIONS

We have determined the Fe isotope equilibrium fractionation between $Fe(II)_{aq}$ and mackinawite at 2°C and 25°C using the three-isotope method. Equilibrium fractionation $\Delta^{56}Fe_{Fe(II)-FeS}$ is -0.52 ± 0.16 ‰ at 2°C and -0.33 ± 0.12 ‰ at 25°C and is equivalent to the distribution between the species Fe^{2+}_{aq} and FeS_m ($\Delta^{56}Fe_{Fe2+-FeS}$). Fractionations produce ^{56}Fe enriched mackinawite and ^{56}Fe depleted dissolved Fe(II). Our results contrast with the kinetic fractionation of $\Delta^{56}Fe_{Fe(II)-FeS}$ = +0.85 to +0.30 ‰ determined by (Butler et al., 2005) with which mackinawite remains depleted even after long term ageing. This means that depending on the degree of FeS_m precipitation from solution, and the degree of isotope exchange during equilibration, FeS_m displays $\delta^{56}Fe$ values in a ~ 1.4 ‰ range. At low temperatures, equilibrium is not reached in periods of less than years. This means that in natural systems, FeS_m is likely to be depleted with regard to its equilibrium value and record a kinetic signature. Further experiments are required to assess the mechanisms responsible for the Fe isotope exchange between aqueous and solid phases.

Our experimental predictions are significantly below the calculated fractionations for the hexagonal Fe(II) monosulphide troilite. There is no obvious evidence why troilite and mackinawite should produce similar β-factors.

Here, we provide the first experimentally determined equilibrium numbers for any metal sulphides. This work is fundamental to isolate and understand each step of Fe isotope fractionations during the formation of pyrite under diagenetic conditions. Further experiments are required to investigate the Fe isotope fractionations occurring in the neutral to alkaline region, where $Fe(II)_{aq}$ speciation is dominated by the clusters FeS^0_{aq}. However, we predict that the fractionation between

FeS^0_{aq} and FeS_m will be small. Experimental isotopic studies in this system would be helpful in further elucidating the roles of the aqueous sulphide clusters in the nucleation of solid phases from solution.

ACKNOWLEDGEMENTS

We are thankful to Alan Matthews, Veniamin Polyakov, Marek Pękala and two anonymous reviewers for constructive discussions that helped to improve substantially the experimental set up and the manuscript. We also thank Kathleen Keefe and Vincent Gallagher for technical support. This work was funded by an ECOSSE PhD studentship to RG and NERC research grant NE/E003958/1 to IBB.

REFERENCES

Anbar A. D. (2004) Iron stable isotopes: beyond biosignatures. *Earth and Planetary Science Letters* **217**, 223-236.

Anbar A. D., Jarzecki A. A., and Spiro T. G. (2005) Theoretical investigation of iron isotope fractionation between $Fe(H_2O)_6^{3+}$ and $Fe(H_2O)_6^{2+}$: Implication for iron stable isotope geochemistry. *Geochim. Cosmochim. Acta* **69**(4), 825-837.

Anbar A. D., Roe J. E., Barling J., and Nealson K. H. (2000) Nonbiological fractionation of iron isotopes. *Science* **288**, 126-128.

Anbar A. D. and Rouxel O. (2007) Metal Stable Isotopes in Paleoceanography. *Annu. Rev. Earth Planet. Sci.* **35**, 717–746.

Archer C. (2007) The application of transition metal isotope systems to biogeochemical studies of the early Earth. PhD thesis. Royal Holloway University London.

Archer C. and Vance D. (2006) Coupled Fe and S isotope evidence for Archean microbial Fe(III) and sulphate reduction. *Geology* **34**, 153-156.

Beard B. and Johnson C. (2004) Fe Isotope Variations in the Modern and Ancient Earth and Other Planetary Bodies. *Reviews in Mineralogy & Geochemistry* **55**, 319-357.

Beard B. L., Handler R. M., Scherer M. M., Wu L., Czaja A. D., Heimann A., and Johnson C. M. (2010) Iron isotope fractionation between aqueous ferrous iron and goethite. *Earth and Planetary Science Letters* **295**(1-2), 241-250.

Beard B. L., Johnson C. M., Cox L., Nealson K. H., and Aguilar C. (1999) Iron isotope biosignatures. *Science* **285**, 1889-1892.

Beard B. L., Johnson C. M., Skulan J. L., Nealson K. H., Cox L., and Sun H. (2003) Application of Fe isotopes to tracing the geochemical and biological cycling of Fe. *Chem. Geol.* **195**, 87-117.

Bennett S.A., Rouxel O., Schmidt K., Garbe-Schonberg D., Statham P.J., and German C. (2009) Iron isotope fractionation in a buoyant hydrothermal plume, 5°S Mid-Atlantic Ridge. *Geoch. Cosmochim. Acta* **73**, 5619-5634.

Berner R. A. (1981) A New Geochemical Classification of Sedimentary Environments. *J. Sediment. Research* **51**.

Blanchard M., Poitrasson F., Méheut M., Lazzeri M., Mauri F., and Balan E. (2009) Iron isotope fractionation between pyrite (FeS2), hematite (Fe2O3) and siderite (FeCO3): A first-principles density functional theory study. *Geochimica et Cosmochimica Acta* **73**(21), 6565-6578.

Borradaile G. (2003) Statistics of Earth Science Data. Springer-Verlag.

Böttcher M. E., Smock A. M., and Cypionka H. (1998) Sulfur isotope fractionation during experimental precipitation of iron(II) and manganese(II) sulphide at room temperature. *Chemical Geology* **146**(3-4), 127-134.

Brantley S. L., Liermann L., and Bullen T. D. (2001) Fractionation of Fe isotopes by soil microbes and organic acids. *Geology* **29**(6), 535-538.

Brantley S. L., Liermann L. J., Guynn R. L., Anbar A., Icopini G. A., and Barling J. (2004) Fe isotopic fractionation during mineral dissolution with and without bacteria. *Geochimica. Cosmochim. Acta* **68**, 3189–3204.

Bullen T. D., White A. F., Childs C. W., Vivit D. V., and Schulz M. S. (2001) Demonstration of significant abiotic ion isotope fractionation. *Geology* **29**, 699-702.

Butler I. B., Archer C., Vance D., Oldroyd A., and Rickard D. (2005) Fe isotope fractionation on FeS formation in ambient aqueous solution. *Earth and Planet. Science Letters* **236**(430-442).

Butler I. B., Schoonen M. A. A., and Rickard D. T. (1994) Removal of dissolved oxygen from water: A comparison of four common techniques. *Talanta* **41**(2), 211-215.

Canfield D. E., Raiswell R., and Bottrell S. H. (1992) The reactivity of sedimentary iron minerals toward sulphide. *American Journal of Science* **292**, 659-683

Criss R. E. (1999) Principles of stable isotope distribution. *Oxford University Press, New York*, 244pp.

Croal L. R., Johnson C. M., Beard B. L., and Newman D. K. (2004) Iron isotope fractionation by Fe(II)-oxidizing photoautotrophic bacteria. . *Geochim Cosmochim Acta* **68**, 1127-1242.

Dauphas N. and Rouxel O. (2006) Mass Spectrometry and natural variations of iron isotopes. *Mass Spectrometry Reviews* **25**, 515-550.

Dideriksen K, Baker J,A, and Stipp S.L.S. (2008) Equilibrium Fe isotope fractionation between inorganic aqueous Fe(III) and the siderophore complex, Fe(III)-desferrioxamine B. *Earth Planet. Sci. Lett.* **269**, 280-290.

Dyrssen D., Kremling, K. (1990) Increasing hydrogen sulphide concentration and race metal behaviour in the anoxic Baltic waters. *Marine Chemistry* **30**, 193-204.

Ehrlich S., Butler I., Halicz L., Rickard D., Oldroyd A., and Matthews A. (2004) Experimental study of the copper isotope fractionation between aqueous Cu(II) and covellite, CuS. *Chemical Geology* **209**(3-4), 259-269.

Ellam R.M. (2006) New constraints on the petrogenesis of the Nuanetsi picrite basalts from Pb and Hf isotope data. *EPSL* **245**, 153-161.

Graham C. M. (1981) Experimental hydrogen isotope studies III: Diffusion of hydrogen in hydrous minerals, and stable isotope exchange in metamorphic rocks. *Contributions to Mineralogy and Petrology* **76**(2), 216-228.

Guilbaud R., Butler I.B., Ellam R.M., and Rickard D. (2010a) Fe isotope exchange between Fe(II)aq and nanoparticulate mackinawite (FeSm) during nanoparticle growth. *Earth Planet. Sci. Lett.* **300**, 174-183.

Guilbaud R., Ellam R. M., Butler I. B., Gallagher V., and Keefe K. (2010b) A procedural development for the analysis of $^{56/54}$Fe and $^{57/54}$Fe isotope ratios with new generation IsoProbe MC-ICP-MS. *J. Anal. At. Spectrom.* DOI: 10.1039/c004876c.

Handler R. M., Beard B. L., Johnson C. M., and Scherer M. M. (2009) Atom Exchange between Aqueous Fe(II) and Goethite: An Fe Isotope Tracer Study. *Environmental Science & Technology* **43**(4), 1102-1107.

Hill P. S. and Schauble E. A. (2008) Modeling the effects of bond environment on equilibrium iron isotope fractionation in ferric aquo-chloro complexes. *Geochimica et Cosmochimica Acta* **72**(8), 1939-1958.

Holland H. D. (1984) The chemical evolution of the atmosphere and oceans. *New York: Princeton University Press.*

Huang F., Zhang H., and Banfield J. F. (2003) Two-Stage Crystal-Growth Kinetics Observed during Hydrothermal Coarsening of Nanocrystalline ZnS. *Nano Letters* **3**(3), 373-378.

Icopini G. A., Anbar A. D., Ruebush S. S., Tien M., and Brantley S. L. (2004) Iron isotope fractionation during microbial reduction of iron: The importance of adsorption. . *Geology* **32**, 205-208.

Jang J.-H., Mathur R., Liermann L. J., Ruebush S., and Brantley S. L. (2008) An iron isotope signature related to electron transfer between aqueous ferrous iron and goethite. *Chemical Geology* **250**(1-4), 40-48.

Jarzecki A. A., Anbar A. D., and Spiro T. G. (2004) DFT Analysis of $Fe(H_2O)_6^{3+}$ and $Fe(H_2O)_6^{2+}$ Structure and Vibrations; Implication for Isotope Fractionation. *J. Phys. Chem. A.* **108**, 2726-2732.

Jeong H. Y., Lee J. H., and Hayes K. F. (2008) Characterization of synthetic nanocrystalline mackinawite: Crystal structure, particle size, and specific surface area. *Geochimica et Cosmochimica Acta* **72**(2), 493-505.

Johnson C. M., Beard B. L. and Roden E. E. (2008) The iron isotope fingerprints of redox and biogeochemical cycles in modern and ancient Earth. *Annu. Rev. Earth Planet. Sci.* **36**, 457–93.

Johnson C. M., Beard B. L., Roden E. E., Newman D. K., and Nealson K. H. (2004) Isotopic Constraints on Biochemical Cycling of Fe. *Reviews in Mineralogy & Geochemistry* **55**, 359-408.

Johnson C. M., Beard B. L., Welch S., Croal L., Newman D., and Nealson K. (2005) Experimental constraints on Fe isotope fractionations during biogeochemical cycling of Fe. *Geochim. Cosmochim. Acta* **66**, A371.

Johnson C. M., Skulan J. L., Beard B. L., Sun H., Nealson K. H., and Braterman P. S. (2002) Isotopic fractionation between Fe(III) and Fe(II) in aqueous solutions. *Earth and Planetary Science Letters* **195**(1-2), 141-153.

Ludwig K. R. (1980) Calculation of uncertainties of U-Pb isotope data. *Earth. Planet. Sc. Lett.* **46**, 212-220.

Luther G. W. and Rickard D. T. (2005) Metal sulphide cluster complexes and their biogeochemical importance in the environment. *Journal of Nanoparticle Research* **7**, 212-220.

Matsuhisa Y., Goldsmith J. R., and Clayton R. N. (1978) Mechanisms of hydrothermal crystallization of quartz at 250°C and 15 kbar. *Geochimica et Cosmochimica Acta* **42**(2), 173-182.

Matsuhisa Y., Goldsmith J. R., and Clayton R. N. (1979) Oxygen isotopic fractionation in the system quartz-albite-anorthite-water. *Geochimica et Cosmochimica Acta* **43**(7), 1131-1140.

Matthews A., Goldsmith J. R., and Clayton R. N. (1983a) On the mechanisms and kinetics of oxygen isotope exchange in quartz and feldspars at elevated temperatures and pressures. *Geol. Soc. Am. Bul.* **94**, 396-412.

Matthews A., Goldsmith J. R., and Clayton R. N. (1983b) Oxygen isotope fractionation involving pyroxenex: the calibration of mineral-pair geothermometers. *Geochim. Cosmochim. Acta* **47**, 631-644.

Matthews A., Morgans-Bell H. S., Emmanuel S., Jenkyns H. C., Erel Y., and Halicz L. (2004) Controls on iron-isotope fractionation in organic-rich sediments (Kimmeridge Clay, Upper Jurassic, Southern England). *Geochimica et Cosmochimica Acta* **68**(14), 3107-3123.

McAnena A., Severmann S., and Poulton S. W. (2009) Abiotic Fe isotope fractionation during sulphide mediated reductive dissolution of Fe oxide minerals. *Goldschmidt Conference Abstracts*.

Michel F. M., Antao S. M., Chupas P. J., Lee P. L., Parise J. B. and Schoonen M. A. A. (2005) Short- to medium- range atomic order and crystallite size of the initial FeS precipitate from pair distribution function analysis. *Chem. Mater.* **17**, 6246-6255.

Michel F.M., Ehm L., Antao S.M., Lee P.L., Chupas P.J., Liu G., Strongin D.R., Schoonen M.A.A., Phillips B.L., and Parise J.B. (2007) The Structure of Ferrihydrite, a Nanocrystalline Material. *Science* **316**, 1726 -1729.

Mikutta C., Wiederhold J.G., Cirpka O.A., Hofstetter T.B., Bourdon B., and Gunten U.V. (2009). Iron isotope fractionation and atom exchange during sorption of ferrous iron to mineral surfaces. *Geochimica et Cosmochimica Acta* **73**, 1795-1812.

Ohfuji H. and Rickard D. (2006) High resolution transmission electron microscopic study of synthetic nanocrystalline mackinawite *Earth and Planet. Science Letters* **241**, 227.

Pankow J. F. and Morgan J. J. (1980) Dissolution of Tetragonal Ferrous Sulphide (Mackinawite) in Anoxic Aqueous Systems. 2. Implications for the Cycling of Iron, Sulfur, and Trace Metals. *Environmental Engineering Science* **14**, 183.

Polyakov V. B., Clayton R. N., Horita J., and Mineev S. D. (2007) Equilibrium iron isotope fractionation factors of minerals: Reevaluation from the data of nuclear inelastic resonant X-ray scattering and Mössbauer spectroscopy. *Geochimica et Cosmochimica Acta* **71**(15), 3833-3846.

Polyakov V. B. and Mineev S. D. (2000) The use of Mossbauer spectroscopy in stable isotope geochemistry. *Geochim Cosmochim Acta* **64**, 849-865.

Poulson R., Johnson C., and Beard B. (2005) Iron isotope exchange kinetics at the nanoparticulate ferrihydrite surface. *American Mineralogist* **90**, 758-763.

Poulton S. W. and Raiswell R. (2002) The low-temperature geochemical cycle of iron: From continental fluxes to marine sediment deposition. *Am J Sci* **302**(9), 774-805.

Pyzik A. J. and Sommer S. E. (1981) Sedimentary iron monosulphides: kinetics and mechanisms of formation. *Geochim. Cosmochim. Acta* **45**(687-698).

Raiswell R. and Berner R. A. (1985) Pyrite formation in euxinic and semi-euxinic sediments. *Am. J. Sci.* **285**, 710-724.

Raiswell R. and Canfield D. E. (1998) Sources of iron for pyrite formation in marine sediments. *Am J Sci* **298**(3), 219-245.

Rickard D. (1974) Kinetics and mechanisms of the sulfidation of goethite. *Am. J. Sci.* **274**, 941-952.

Rickard D. (1995) Kinetics of FeS precipitation: Part 1. Competing reaction mechanisms. *Geochim. Cosmochim. Acta* **59**, 4367– 4379.

Rickard D. (2006) The solubility of FeS. *Geochimica et Cosmochimica Acta* **70**(23), 5779-5789.

Rickard D., Griffith A., Oldroyd A., Butler I. B., Lopez-Capel E., Manning D. A., and Apperley D. C. (2006) The composition of nanoparticulate mackinawite, tetragonal iron (II) monosulphide. *Chem. Geol.* **235**(286).

Rickard D. and Luther G. W., III. (1997) Kinetics of pyrite formation by the H_2S oxidation of iron(II) monosulphide in aqueous solutions between 25°C and 125°C: The mechanism. *Geochimica Cosmochimica Acta* **61**, 135-147.

Rickard D. and Luther G. W., III. (2007) Chemistry of Iron Sulphides. *Chem. Rev.* **107**, 514-562.

Rickard D. and Morse J. W. (2005) Acid Volatile Sulphide (AVS). *Marine Chemistry* **97**, 141-197.

Rickard D. and Sjoberg E. L. (1983) Mixed kinetic control of calcite dissolution rates. *American Journal of Science* **283**, 815-830.

Rouxel O. J., Bekker A., and Edwards K. J. (2005) Iron isotope constraints on the Archean and Paleoproterozoic ocean redox state. *Science* **307**, 1088-1090.

Rouxel O., Shanks III W.C., Bach W., and Edwards K.J. (2008) Integrated Fe- and S-isotope study of seafloor hydrothermal vents at East Pacific Rise 9-10°N. *Chemical Geology* **252**, 214-227.

Schauble E. A., Ghosh P., and Eiler J. M. (2006) Preferential formation of 13C-18O bonds in carbonate minerals, estimated using first-principles lattice dynamics. *Geochimica et Cosmochimica Acta* **70**(10), 2510-2529.

Schauble E. A., Rossman G. R., and Taylor H. P. (2001) Theoretical estimates of equilibrium Fe-isotope fractionations from vibrational spectroscopy. *Geochimica et Cosmochimica Acta* **65**(15), 2487-2497.

Schuessler J.A., Schoenberg R., Behrens H., and Blanckenburg F.V. (2007) The experimental calibration of the iron isotope fractionation factor between pyrrhotite and peralkaline rhyolitic melt. *Geochimica et Cosmochimica Acta* **71**, 417-433.

Severmann S., Johnson C. M., Beard B. L., and McManus J. (2006) The effect of early diagenesis on the Fe isotope compositions of porewaters and authigenic minerals in continental margin sediments. *Geochim Cosmochim Acta* **70**, 2006–2022.

Shahar A., Young E. D., and Manning C. E. (2008) Equilibrium high-temperature Fe isotope fractionation between fayalite and magnetite: An experimental calibration. *Earth and Planet. Science Letters* **268**, 330–338.

Skulan J. L., Beard B. L., and Johnson C. M. (2002) Kinetic and equilibrium Fe isotope fractionation between aqueous Fe(III) and hematite. *Geochim. Cosmochim. Acta* **66**, 2995-3015.

Smith R. M., Martell, A.E. (1976) Critical Stability Constants, v.4, Inorganic Complexes. *Plenum Press*.

Teutsch N., von Gunten U., Porcelli D., Cirpka O. A., and Halliday A. N. (2005) Adsorption as a cause for iron isotope fractionation in reduced groundwater. *Geochim Cosmochim Acta* **69**, 4175-4185.

Theberge S. M. and Luther G.W., III. (1997) Determination of the electrochemical properties of a soluble aqueous FeS cluster present in sulfidic systems. *Aquatic Geochemistry* **3**, 191-211.

Turner D. R., Whitfield M., and Dickson A. G. (1981) The equilibrium speciation of dissolved components in freshwater and sea water at 25°C and 1 atm pressure. *Geochim Cosmochim Acta* **45**, 855-881.

Waychunas G. A., Kim C. S., and Banfield J. F. (2005) Nanoparticulate Iron Oxide Minerals in Soils and Sediments: Unique Properties and Contaminant Scavenging Mechanisms. *Journal of Nanoparticle Research* **7**(4), 409-433.

Wei D. and Osseo-Asare K. (1996) Particulate pyrite formation by the $Fe3^{+}/HS^{-}$ reaction in aqueous solutions: effects of solution composition. *Colloids and surfaces A: Physicochemical and Engineering Aspects* **118**, 51-61.

Welch S. A., Beard B. L., Johnson C. M., and Baterman P. S. (2003) Kinetic and equilibrium Fe isotope fractionation between aqueous Fe(II) and Fe(III). *Geochim. Cosmochim. Acta* **67**, 4231-4250.

Wells M. L., Price N. M., and Bruland K. W. (1995) Iron chemistry in seawater and its relationship to phytoplankton: a workshop report. *Mar. Chem.* **48**, 157-182.

Wiederhold J.G., Kraemer S.M., Teutsch N., Borer P.M., Halliday A.N., and Kretzschmar R. (2006). Iron Isotope Fractionation during Proton-Promoted, Ligand-Controlled, and Reductive Dissolution of Goethite. *Environmental Science & Technology* **40**, 3787-3793.

Wiesli R. A., Beard B. L., and C.M. J. (2004) Experimental determination of Fe isotope fractionation between aqueous Fe(II), siderite and "green rust" in abiotic systems. *Chem. Geol.* **211**, 343-362.

Wolthers M., van der Gaast S. J., and Rickard D. (2003) The structure of distored mackinawite. *Am. Mineral.* **88**, 2007.

Wolthers M., van der Gaast S., Charlet L., and Rickard D. (2005). A surface and structural model describing the environmental reactivity of disordered mackinawite. *Am. Mineral.* **88**, 2007-2015.

Yamaguchi K. E., Johnson C. M., Beard B. L., and Ohmoto H. (2005) Biogeochemical cycling of iron in the Archean-Paleoproterozoic Earth: Constraints from iron isotope variations in sedimentary rocks from the Kaapvaal and Pilbara Cratons. *Chem. Geol.* **218**, 135-169.

	2°C experiment									25°C experiment							
Sample	Experiment duration (h)	δ^{56}Fe Fe(II) ‰	δ^{57}Fe Fe(II) ‰	δ^{56}Fe FeSm ‰	δ^{57}Fe FeSm ‰	FeS fraction	mass balance δ^{56}Fe	mass balance δ^{57}Fe	*F* 2°C	δ^{56}Fe Fe(II) ‰	δ^{57}Fe Fe(II) ‰	δ^{56}Fe FeSm ‰	δ^{57}Fe FeSm ‰	FeS fraction	mass balance δ^{56}Fe	mass balance δ^{57}Fe	*F* 25°C
Eq-0	0	0.20	0.20	308.30	5.80	0.425	112.79	2.58	0.00	0.20	0.20	308.30	5.80	0.425	112.79	2.58	0.00
Eq-1-A	24	25.00	0.67	243.34	4.97	0.426	108.37	2.50	0.31	55.05	1.62	171.68	4.00	0.440	103.60	2.42	0.54
Eq-1-B	24	24.56	0.67	234.51	4.85	0.446	105.05	2.45	0.36	56.29	1.67	169.06	4.11	0.425	101.64	2.43	0.55
Eq-2-A	48	33.65	0.89	229.16	4.62	0.423	108.82	2.48	0.38	66.08	1.88	143.38	3.69	0.430	97.71	2.40	0.65
Eq-2-B	48	29.57	0.89	217.66	4.56	0.427	102.45	2.45	0.44	68.29	1.88	146.56	3.83	0.446	101.90	2.43	0.67
Eq-3-A	96	44.38	1.12	201.43	4.21	0.425	106.19	2.43	0.52	71.83	1.92	136.66	3.50	0.451	100.19	2.43	0.70
Eq-3-B	96	43.99	1.12	192.04	4.19	0.427	102.50	2.42	0.56	78.24	1.89	141.60	3.74	0.423	104.35	2.52	0.77
Eq-4-A	144	51.03	1.25	180.50	4.05	0.430	102.68	2.44	0.62	77.97	2.02	129.75	3.23	0.440	100.21	2.19	0.76
Eq-4-B	144	50.62	1.25	178.82	4.05	0.425	101.79	2.44	0.63	77.43	1.98	130.86	3.25	0.425	99.55	2.63	0.76
Eq-5-A	432	60.66	1.28	158.15	3.68	0.422	100.16	2.30	0.73	81.73	2.12	120.41	3.33	0.440	98.45	2.35	0.80
Eq-5-B	432	58.63	1.30	163.87	3.94	0.425	101.11	2.42	0.70	79.98	2.07	118.79	3.22	0.440	96.74	2.40	0.78
Eq-6-A	768	65.77	1.56	150.23	3.62	0.425	100.21	2.44	0.77	82.69	2.13	118.19	3.20	0.446	98.25	2.44	0.81
Eq-6-B	768	66.26	1.51	151.92	3.61	0.423	101.18	2.40	0.76	83.21	2.15	119.52	3.21	0.485	100.56	2.12	0.82
Eq-7-A	2880	-	-	-	-	-	-	-	-	86.79	2.20	109.73	3.24	0.425	96.43	2.60	0.85
	Predicted equilibirum		2.20		2.96						2.57		3.05				
	upper limit		2.32		3.06						2.66		3.15				
	lower limit		2.08		2.85						2.49		2.95				
	Δ^{57}Fe(II)-FeSm ‰		***0.76***								***0.48***						
			±0.24								±0.17						
	Δ^{56}Fe(II)-FeSm ‰		***0.51***								***0.32***						
			±0.16								±0.12						

Table 1: Experimental conditions and isotopic analysis. Analytical precision of the isotopic data is the 2standard deviation (2σ) of the external standard (Baker™ Fe solution) and was ± 0.08 ‰ and ± 0.17 ‰ for $\delta^{56}Fe$ and $\delta^{57}Fe$ respectively. $\Delta^{56}Fe_{Fe(II)\text{-}FeS}$ and $\Delta^{56}Fe_{Fe(II)\text{-}FeS}$ were calculated from the difference between the predicted Fe isotope compositions of both FeS_m and $Fe(II)_{aq}$ at equilibrium. Errors on $\Delta^{56}Fe_{FeS\text{-}Fe(II)}$ are determined by the intercepts between the 95% confidence envelopes and the secondary fractionation line from Eqs. 3 and 4. The mass balance and the extent of reaction *F* were calculated from Eqs. 5 and 6, respectively. The FeS fraction represent the Fe_{FeS}/Fe_{total} ratio, for which $[Fe]_{FeS}$ and $[Fe]_{Fe(II)}$ were measured spectrophotometrically at the end of each experiment.

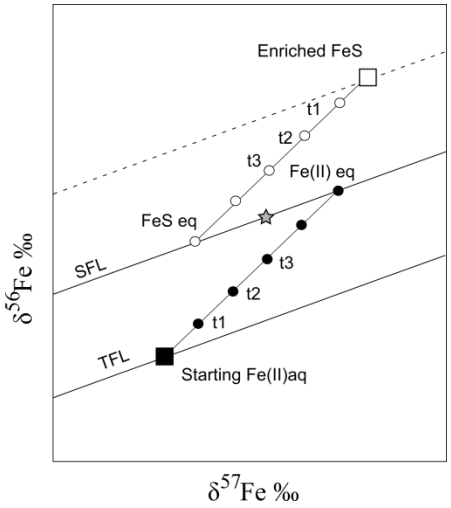

Fig. 1: Principle of the three isotope method. Starting materials are represented by squares. Starting $Fe(II)_{aq}$ lies on the terrestrial fractionation line (TFL), enriched ^{56}FeS has a composition shifted from the TFL. Circles represent the evolution of isotopic compositions of both phases with time. When the system reaches isotopic equilibrium, the final compositions will lie on the secondary fractionation line (SFL). If $\Delta_{equilibirum}$ = 0‰, final compositions will meet at the bulk composition represented by a star. If $\Delta_{equilibirum} \neq 0$‰, it equals the difference between $\delta_{Fe(II),\ equilibrium}$ and $\delta_{FeS,\ equilibrium}$.

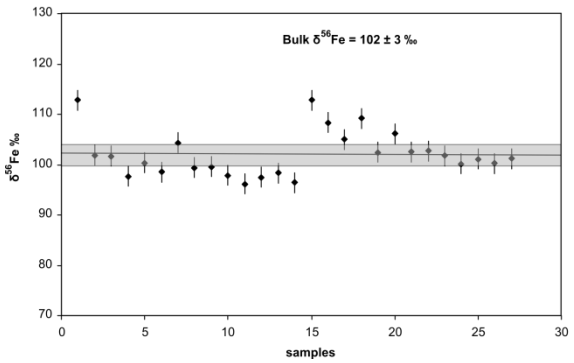

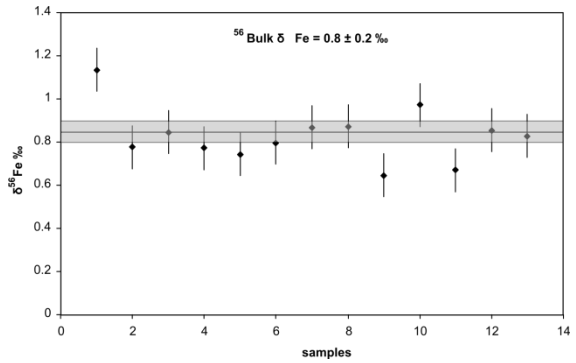

Fig. 2: Experimental mass balance for the $\delta^{56}Fe_{FeS}$ ~ 308 ‰ and $\delta^{56}Fe_{FeS}$ ~ 2.6 ‰ starting experiments, calculated from Eq. 5. Grey areas represent the experimental external precision based on the reproducibility of the replicates.

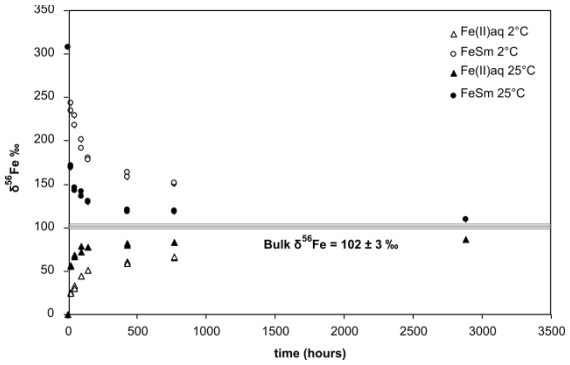

Fig. 3: Time evolution of Fe isotope compositions of FeS_m (circles) and $Fe(II)_{aq}$ (triangles) at 25°C (filled signs) and 2°C (open signs). 2°C experiments were stopped after one month. 25°C experiments were stopped after four months. The grey area is the bulk composition of the system including errors.

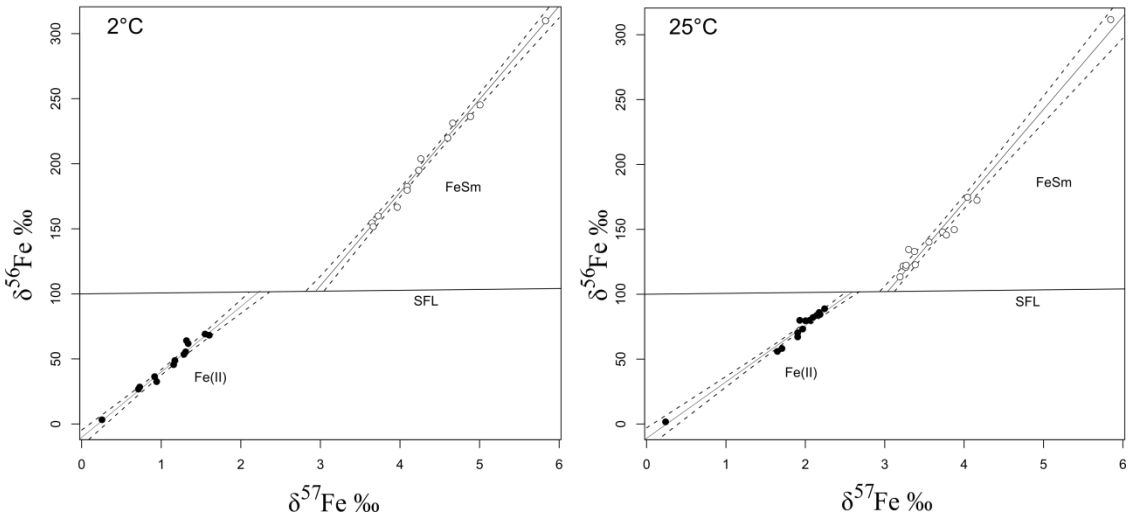

Fig. 4: Three isotope plots starting with $\delta^{56}Fe_{FeS}$ ~ 308 ‰ and predicted equilibrium Fe isotope fractionations on the SFL between FeS_m (open circles) and $Fe(II)_{aq}$ (filled circles). $\Delta^{56}Fe_{Fe(II)\text{-}FeS}$ is the difference between the intersections of the regression lines with the SFL. 95 % confidence envelopes are calculated from Eq. 3.

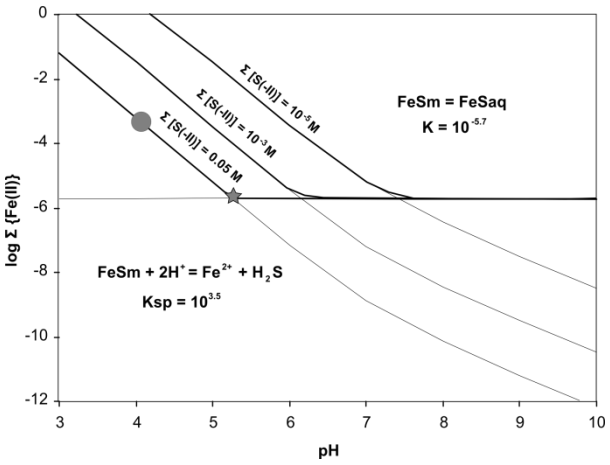

Fig. 5: Modified from Rickard (2006). Total dissolved Fe(II) activity in equilibrium with FeS_m for various total [S(-II)] (bold lines). pH dependent and independent reactions are showed as fine lines. Our experiment corresponds to the region marked by a circle. The grey star represents the limit at which FeS_{aq} becomes the dominant $Fe(II)_{aq}$ species, as opposed to Fe^{2+} (pH ~ 5.2 for Σ[S(-II)] = 0.05 M).

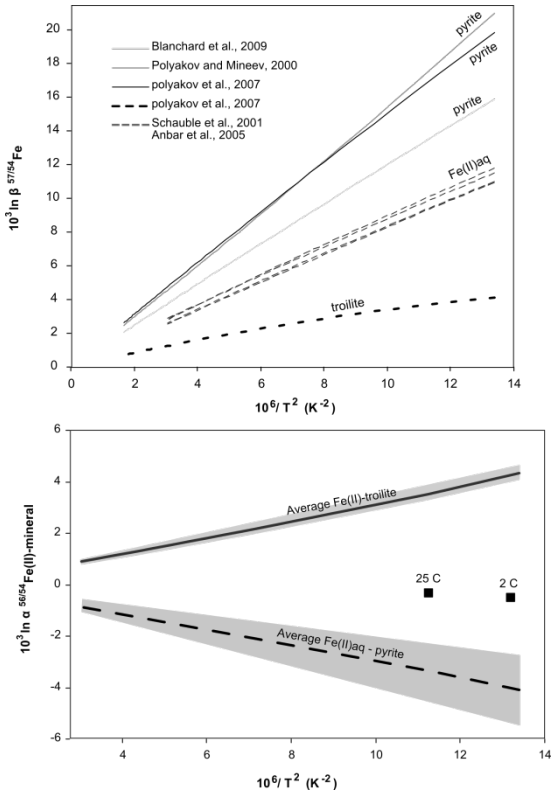

Fig. 6: A: β-factors for troilite (bold-dot line, Polyakov et al., 2007), $Fe(II)_{aq}$ (grey dot lines, Schauble et al., 2001; Anbar et al., 2005) and pyrite (plain lines, Blanchard et al., 2009; Ployakov and Mineev, 2000; Polyakov et al., 2007). B: Temperature dependence of $\Delta^{56}Fe_{Fe(II)\text{-mineral}}$ for average pyrite (bold line), average troilite (dot-line) and our experimental results (filled squares) calculated from the β-factors from A. Grey areas correspond to the uncertainties from calculations.

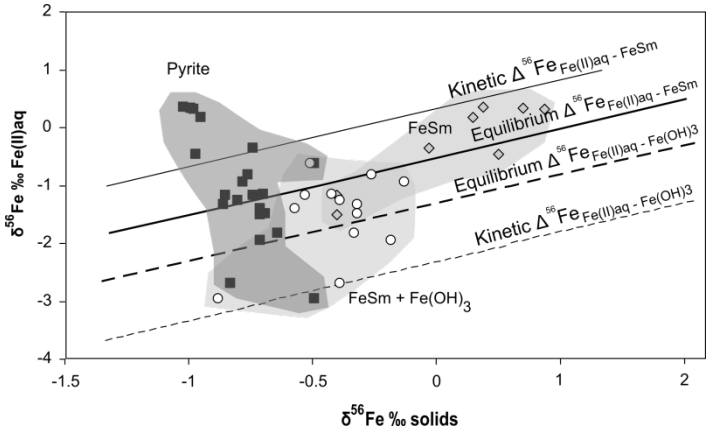

Fig. 7: Plot of the isotopic compositions of pore water versus the solid highly reactive iron phases, modified after Johnson et al. (2008). Data for pyrite (filled squares) and HCl extrated phases (grey diamonds and open circles) are from Severmann et al. (2006). Compositions for FeS_m were derived from HCl extraction data where $Fe(II)_{HCl}$ > 80%, as suggested by Johnson et al. (2008). Kinetic $\Delta^{56}Fe_{Fe(II)aq\text{-}FeSm}$ are from Butler et al. (2005). We used our 2°C values for equilibrium $\Delta^{56}Fe_{Fe(II)aq\text{-}FeSm}$. Kinetic and equilibrium $\Delta^{56}Fe_{Fe(II)aq\text{-}Fe(OH)3}$ are from Johnson et al. (2004).